Int. J. Heat Mass Transfer. Vol. 31, No. 2, pp. 219–227, 1988
Printed in Great Britain

0017–9310/88 $3.00 + 0.00

Critical heat flux on a disk heater cooled by a circular jet of saturated liquid impinging at the center

Y. KATTO
Department of Mechanical Engineering, Nihon University, Kanda-Surugadai, Chiyoda-ku, Tokyo, Japan

and

S. YOKOYA
Department of Mechanical Engineering, University of Tokyo, Hongo, Bunkyo-ku, Tokyo, Japan

(*Received* 10 *April* 1987)

Abstract—The existing data of critical heat flux (CHF) on a disk heater cooled by a liquid jet have been analyzed, and a generalized correlation of the data is presented, covering the vapor-to-liquid density ratio $\rho_v/\rho_l = 0.000624$–0.189 and disk-to-nozzle diameter ratio $d/d_N = 3.9$–53.9. An empirical method is also presented to estimate the limit at which CHF begins to deviate from the normal state. Finally, it is shown that the system of a disk heater with an impinging jet has similarities in the character of CHF to the system of a heated cylinder in a cross flow.

1. INTRODUCTION

CRITICAL heat flux (CHF) on a disk heater cooled by an impinging jet, such as schematically illustrated in Fig. 1, is an important phenomenon, not only having a close relation to a means for heat removal of local high cooling rate but also having a potentiality to give us some fundamental information on the CHF mechanism. The present study restricts consideration to a basic system, where the liquid droplets created by boiling at high heat fluxes (Fig. 1) do not return to the disk surface.

Measurement of CHF in this jet–disk system began with water at atmospheric pressure in a narrow range of nozzle exit velocities $u = 1.2$–3.0 m s^{-1} employing a disk heater of diameter $d = 10$ mm combined with nozzles of diameter $d_N = 0.7$–1.6 mm [1]. Reference [2] subsequently measured CHF of water at atmospheric pressure over a very wide range of velocities $u = 5.3$–60.0 m s^{-1} for a square heater of 8×8 mm (that is equivalent to a disk heater of $d = \sqrt{(2 \times 8^2)}$ mm). Reference [3] then moved to more systematic experiments with water and R-113 at atmospheric pressure, extending the range of vapor–liquid density ratio to $\rho_v/\rho_l = 0.000624$–0.00495. Reference [4] carried out experiments with R-12 (0.60–2.79 MPa) as well as water and R-113, extending the experimental range of density ratio up to $\rho_v/\rho_l = 0.000624$–0.189 at a stroke.

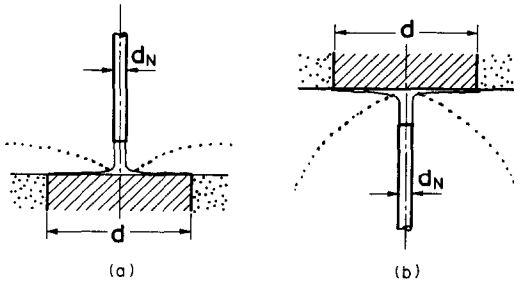

FIG. 1. A disk heater cooled by a liquid jet: (a) upward-facing disk system; (b) downward-facing disk system.

Employing disks of diameter $d \leqslant 25.5$ mm, ref. [5] extended the range of diameter ratio to $d/d_N = 5.0$–36.4, while Katsuta [6], and Katsuta and Kurose [7] carried out experiments of CHF for disks of $d = 15$–25 mm within a rather low velocity range of $u = 0.5$–3.8 m s^{-1}. Meanwhile, ref. [8] improved on the experimental apparatus previously used in ref. [4] doubling the disk diameter, and performed experiments of CHF with water (0.10–0.57 MPa), R-113 (0.10–0.30 MPa), and R-12 (0.57–2.78 MPa). Reference [9] employed downward-facing large disk heaters of $d = 40$ and 60 mm against nozzle diameters of $d_N = 1.1$–4.1 mm ($d/d_N = 9.6$–54.1) for experiments of CHF of water and R-113 at atmospheric pressure in a range of $u = 0.3$–13.7 m s^{-1} including comparatively low velocities. Reference [10], employing the same experimental apparatus as that of ref. [8], made experiments of CHF for disk heaters of $d = 10$–40 mm.

On the other hand, studies on the correlation of experimental data have so far been made following the accumulation of data achieved by the foregoing experiments. Reference [3] analyzed the data of water and R-113 at atmospheric pressure obtained in refs. [1–3] to derive the following generalized correlation:

$$\frac{q_{c0}}{GH_{fg}} = 0.0745\left(\frac{\rho_v}{\rho_l}\right)^{0.275}\left(\frac{\sigma\rho_l}{G^2 d}\right)^{1/3} \quad (1)$$

NOMENCLATURE

d	diameter of disk heater [m]	u	mean velocity of liquid jet at nozzle exit [m s^{-1}].
d_N	diameter of nozzle [m]		
G	mass velocity of liquid jet, $u\rho_l$ [kg m^{-2} s^{-1}]		
H_{fg}	latent heat of evaporation [J kg^{-1}]		
K	coefficient in equation (12) [—]	Greek symbols	
m	exponent in equation (12) [—]	ρ_l	density of liquid [kg m^{-3}]
q_{c0}	critical heat flux for saturated liquid jet [W m^{-2}]	ρ_v	density of vapor [kg m^{-3}]
		σ	surface tension [N m^{-1}].

where q_{c0} is the critical heat flux, G the mass velocity of liquid jet ($G = u\rho_l$), and σ the surface tension. Reference [4] then analyzed data for R-12 in a wide range of ρ_v/ρ_l to present the following tentative correlations:

$$\frac{q_{c0}}{GH_{fg}} = 0.188\left(\frac{\rho_v}{\rho_l}\right)^{0.386}\left(\frac{\sigma\rho_l}{G^2d}\right)^{1/3} \tag{2}$$

$$\frac{q_{c0}}{GH_{fg}} = 1.18\left(\frac{\rho_v}{\rho_l}\right)^{0.386}\left(\frac{\sigma\rho_l}{G^2d}\right)^{1/2} \tag{3}$$

for V and I regimes, respectively. The V regime was assumed as a regime of relatively low G values where q_{c0} was 'variable' with G, while the I regime was a regime of high G values where q_{c0} was 'invariable' with G. The boundary between the two regimes must correspond to the intersecting point of equations (2) and (3), but ref. [4] noted the existence of some data which did not accede to the above-mentioned classification of regimes.

Meanwhile, Monde [5], analyzing the data of water at atmospheric pressure in a wide range of d/d_N, modified equation (1) for the effect of d/d_N as follows:

$$\frac{q_{c0}}{GH_{fg}} = 0.0757\left(\frac{\rho_v}{\rho_l}\right)^{0.275}\left(\frac{\sigma\rho_l}{G^2d}\right)^{1/3}\frac{1}{1+0.00113(d/d_N)^2}. \tag{4}$$

Katsuta and Kurose [7] also analyzed CHF data of their own in a narrow range of mass velocity G to give

$$\frac{q_{c0}}{GH_{fg}} = 0.160\left(\frac{\rho_v}{\rho_l}\right)^{0.3}\left(\frac{\sigma\rho_l}{G^2d}\right)^{1/4}\frac{1}{(d/d_N)^{3/4}}. \tag{5}$$

A little later, relating to the mechanism of CHF, ref. [11] proposed a concept of Critical Liquid Film Thickness on a high-heat-flux nucleate boiling surface. If this concept is applied to the jet–disk system assuming a simple model of liquid flow, the following equation is readily derived employing neither empirical constants nor empirical exponents (cf. ref. [12]):

$$\frac{q_{c0}}{GH_{fg}} = 0.278\left(\frac{\rho_v}{\rho_l}\right)^{0.467}\left(1+\frac{\rho_v}{\rho_l}\right)^{1/3} \times\left[\frac{\sigma\rho_l}{G^2(d-d_N)}\frac{1}{1+d/d_N}\right]^{1/3}. \tag{6}$$

Taking dimensionless groups derived in equation (6) into account, Monde [10, 13] analyzed the existing data of water, R-113, and R-12 to present the following equations to the V and I regime, respectively:

$$\text{V:}\quad \frac{q_{c0}}{GH_{fg}} = 0.280\left(\frac{\rho_v}{\rho_l}\right)^{0.355}\left[\frac{\sigma\rho_l}{G^2(d-d_N)}\right]^{0.343} \times\frac{1}{(1+d/d_N)^{0.364}} \tag{7}$$

$$\text{I:}\quad \frac{q_{c0}}{GH_{fg}} = 0.925\left(\frac{\rho_v}{\rho_l}\right)^{0.534}\left[\frac{\sigma\rho_l}{G^2(d-d_N)}\right]^{0.421} \times\frac{1}{(1+d/d_N)^{0.303}}. \tag{8}$$

Equation (7) was derived mainly from the data of water and R-113, while equation (8) from R-12 data of high ρ_v/ρ_l values obtained at relatively high velocities. No general principle was presented to separate the two regimes quantitatively.

Meanwhile, there is another type of approach to the correlation of data, which is based on the Mechanical Energy Stability Criterion proposed by Lienhard and Eichhorn [14]. First, Lienhard and Eichhorn [15] showed that the data of refs. [2, 3] could be correlated in the following form:

$$\phi\beta/r^{0.725} = \text{function of}\ \beta^3/We \tag{9}$$

where $\phi = q_{c0}/\rho_v H_{fg}u$, $\beta = d/d_N$, $r = \rho_l/\rho_v$, and $We = \rho_l u^2 d/\sigma = G^2 d/\sigma\rho_l$. Lienhard and Hasan [16] then analyzed the new data of ref. [4] as well as the data of refs. [2, 3] to give

$$\frac{\phi\beta}{f(r)} = \left(\frac{\beta^3}{We}\right)^{A(r)} \tag{10}$$

where $f(r)$ and $A(r)$ were determined empirically as functions of r, respectively. Recently, Sharan and Lienhard [17] carried out the analysis of the data of refs. [2–5] to revise equation (10) about the effect of β as follows:

$$\frac{\phi\beta^{1/3}}{f_2(r)} = \left[\frac{1000}{We}\right]^{A_2(r)} \tag{11}$$

where

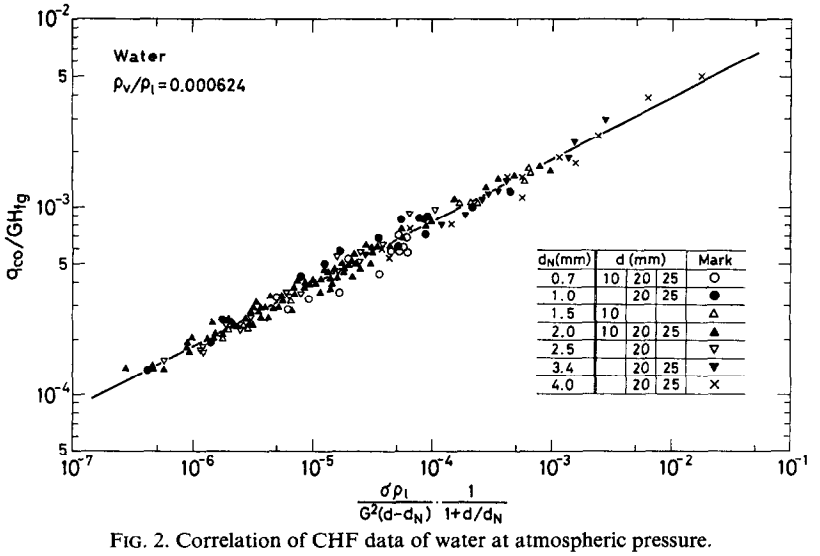

FIG. 2. Correlation of CHF data of water at atmospheric pressure.

$$f_2(r) = 0.00171r + 0.21$$

and

$$A_2(r) = 0.486 + 0.06052(\ln r) - 0.0378(\ln r)^2 + 0.00362(\ln r)^3.$$

The foregoing two independent approaches to the correlation of data assume some aspects incompatible with each other. For example, the Monde correlation is composed of equations (7) and (8) corresponding to two different regimes, while the Sharan and Lienhard correlation is only one equation, equation (11), with an exponent $A_2(r)$ of a rather complicated nature. In the present study, therefore, the existing data is analyzed carefully to derive a new correlation, and the evaluation of the existing two correlations is also attempted on the basis of the new correlation.

2. CORRELATION OF CHF DATA

2.1. *Analysis of data under normal condition*

In coping with the effects of three main parameters of G, d and d_N on critical heat flux q_{c0}, the present analysis starts in on testing the utility of a dimensionless group $\sigma\rho_l/G^2(d-d_N)(1+d/d_N)$ included in equation (6). Figure 2 represents all the existing data of water obtained at atmospheric pressure ($\rho_v/\rho_l = 0.000624$), where q_{c0}/GH_{fg} is plotted against the above-mentioned dimensionless group. It will be noted in Fig. 2 that the experimental data, which have been collected from different sources (refs. [1–5, 8]) covering wide ranges of conditions (u = 0.15–60.0 m s^{-1}, d = 10.0–25.5 mm, d_N = 0.7–4.1 mm, and d/d_N = 5.0–36.4), gather together along a correlation line that is determined by the least squares method. This means that the data in Fig. 2 can be correlated with the following form:

$$\frac{q_{c0}}{GH_{fg}} = K\left[\frac{\sigma\rho_l}{G^2(d-d_N)}\frac{1}{1+d/d_N}\right]^m \qquad (12)$$

where K and m are constants, respectively, for water at atmospheric pressure.

Similarly, Fig. 3 represents the main part of R-113 data obtained at atmospheric pressure ($\rho_v/\rho_l = 0.00495$), and all the data of R-12 at 2.79 MPa ($\rho_v/\rho_l = 0.189$), both displaying the same character as that of Fig. 2. All the correlation lines, determined in the same way as above for various data groups, are presented in Fig. 4, and the data conditions for each correlation line are listed in Table 1. For this analysis, some scattering or irregular data have been eliminated, because it is technically difficult for such data to determine meaningful correlation lines.

The following matters will be noted from Fig. 4.

(1) The main correlation line 3 for R-113 at $\rho_v/\rho_l = 0.00495$ is accompanied by three satellite lines 3′, 3″, and 3‴, where lines 3′ and 3‴ have been obtained from a relatively small number of data, respectively (Table 1). According to Monde [18], this dispersion of data may possibly be related to the effect of impurities such as oils in solution.

(2) Two groups of R-12 data at $\rho_v/\rho_l = 0.0661$ and 0.114 give a couple of correlation lines, respectively; one for the data of d = 20 and 40 mm (lines 8 and 11) and the other for the data of d = 10 mm (lines 8′ and 11′).

(3) Correlation line 12 for $\rho_v/\rho_l = 0.114$ shows a deviation as compared with the locations of line 11 for $\rho_v/\rho_l = 0.114$ and line 13 for $\rho_v/\rho_l = 0.189$.

If viewed from a statistical point, however, correlation lines in Fig. 4 are in order of ρ_v/ρ_l for either the slope or the location. In fact, one can see it clearly in Fig. 5, where the values of K and m in equation (12), determined directly by the least squares method

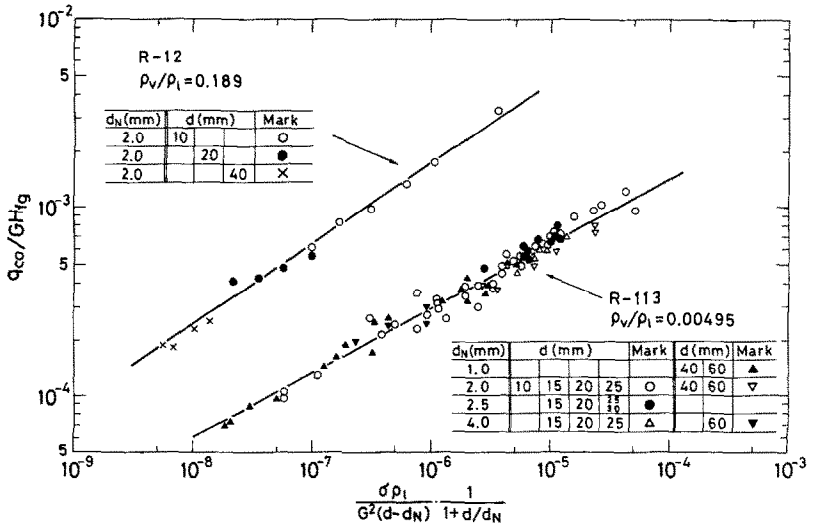

FIG. 3. Correlation of CHF data for R-113 at atmospheric pressure and R-12 at 2.78 MPa.

for each data group, are plotted against ρ_v/ρ_l, respectively.

Now, Fig. 5 reveals that the relative change of m with ρ_v/ρ_l is small as compared with that of K. Hence, it is considered preferable to derive a correlation equation of m first from the 18 data points of m in Fig. 5; and when it is done with the help of the least squares method, the following result is obtained:

$$\left.\begin{aligned} m &= 0.374(\rho_v/\rho_l)^{0.0155} \quad \text{for} \quad \rho_v/\rho_l \leqslant 0.00403 \\ m &= 0.532(\rho_v/\rho_l)^{0.0794} \quad \text{for} \quad \rho_v/\rho_l \geqslant 0.00403. \end{aligned}\right\} \tag{13}$$

Next, assuming a non-linear form of $K = a + b(\rho_v/\rho_l)^c$ in equation (12) with a little difference from that of $f(r)$ in equation (11), and determining the values of a, b and c, by means of the least squares method for all the existing data to the number of 564 (Table 1) on the basis of equation (13) for m, it gives

$$K = 0.0166 + 7.00(\rho_v/\rho_l)^{1.12}. \tag{14}$$

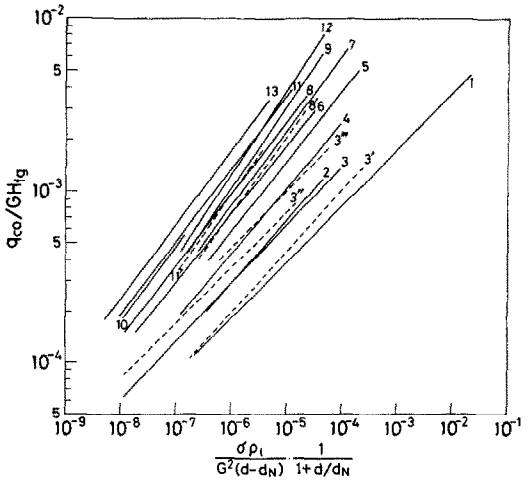

FIG. 4. Correlation lines of CHF data (see Table 1 for conditions of data relating to each line).

Thick solid lines illustrated in Fig. 5 represent equations (13) and (14) thus determined, showing good agreement with the experimental points of m and K, respectively.

2.2. *Applicable limit of equation* (12)

Under a given condition, the flow rate of liquid from a nozzle is reduced excessively, when CHF takes values less than the normal one. This phenomenon has already been noted in the experiments of ref. [1] with an upward-facing disk heater, and the regime to cause such CHF was called the D regime in ref. [4], assuming a simple 'dryout' process of liquid on a heated disk. Figure 6 shows typical examples of CHF data obtained later by Monde and Okuma [9], and Monde [10] for downward-facing disks of large diameters. One can see clearly that as G is reduced, the data points begin to deviate from thick solid lines representing the normal value of CHF which follows the rule of equation (12).

Monde and Okuma [9] analyzed CHF data of water and R-113 at atmospheric pressure in such a special regime for the case of a downward-facing disk (Fig. 1(b)). Employing the Taylor instability critical wavelength for a downward-facing liquid surface, they succeeded in deriving a generalized correlation of such CHF data. In the present study, however, it has been found that this correlation is inapplicable to the data of R-12 such as those illustrated in Fig. 6. In ref. [10], R-12 data of this kind were classified to a newly defined regime of high pressure, which is called the HP regime, but it seems likely that no solid foundation was presented for it.

Meanwhile, Sharan and Lienhard [17] discussed two limiting conditions caused by the effects of viscosity and gravity, suggesting that for the former case, the limit of velocity u is predicted by $d/d_N = 0.5245(ud_N/\nu)^{1/3}$, and for the latter case, by $u/\sqrt{(gd)} \cong 10$. However, when compared with exper-

Table 1. Conditions of data giving the correlation lines in Fig. 4

No.	Fluid	ρ_v/ρ_l	d_N (mm)	d (mm)	d/d_N	Number of data	Sources
1	Water	0.000624	0.7–4.1	10.0–25.5	5.0–36.4	219	[1–5, 8]
2	Water	0.00342	2.0	18.9	9.5	6	[8]
3	R-113	0.00495	1.1–4.1	11.6–60.1	3.9–53.9	105	[3, 6, 9]
3′	R-113	0.00495	2.0–4.1	19.9–40.3	9.6–11.9	18	[8, 9]
3″	R-113	0.00495	1.1–2.5	20.9–40.3	8.4–36.3	52	[3, 9]
3‴	R-113	0.00495	2.0	10.0	5.0	8	[4]
4	R-113	0.0149	2.0	18.9–19.9	9.5–10.0	8	[8]
5	R-12	0.0257	2.0	10.0	5.0	17	[4]
6	R-12	0.0434	2.0	19.9–40.2	10.0–20.1	20	[8, 10]
7	R-12	0.0544	2.0	10.0	5.0	19	[4]
8	R-12	0.0662	2.0	19.9–40.2	10.1–20.1	18	[8, 10]
8′	R-12	0.0662	2.0	10.2	5.1	9	[10]
9	R-12	0.0928	2.0	10.0	5.0	14	[4]
10	R-12	0.0955	2.0	40.2	20.1	6	[10]
11	R-12	0.114	2.0	19.9–40.2	10.0–20.1	16	[8, 10]
11′	R-12	0.114	2.0	10.2	5.1	8	[8]
12	R-12	0.141	2.0	10.0	5.0	7	[4]
13	R-12	0.189	2.0	10.0–40.2	5.0–20.1	14	[4, 8, 10]
					Total	564	

imental data such as in Fig. 6, the predictions are found to work inadequately.

Hence, further studies are needed to get a satisfactory solution to the foregoing problem. Under such circumstances, this paper presents tentatively a purely empirical way to predict the transition point from the normal state, which is based on the following equation:

$$\left(\frac{q_{c0}}{GH_{fg}}\right)_{trans.} = k\frac{1}{(d/d_N)^2} \tag{15}$$

$k = 1$ in equation (15) corresponds to a limiting state that the whole quantity of liquid fed from a nozzle is just dried out due to evaporation on a disk surface; all actual values of k determined from the experimental data of $(q_{c0}/GH_{fg})_{trans.}$ are plotted in Fig. 7. Though not a generalized form, the result of Fig. 7 may be utilized to make rough estimations of $(q_{c0}/GH_{fg})_{trans.}$ through equation (15).

3. DISCUSSION

(1) Average and r.m.s. errors calculated on the basis of the existing data are listed in Table 2 as to predictions of the Monde, the Sharan and Lienhard, and the present correlation. As for the Monde correlation,

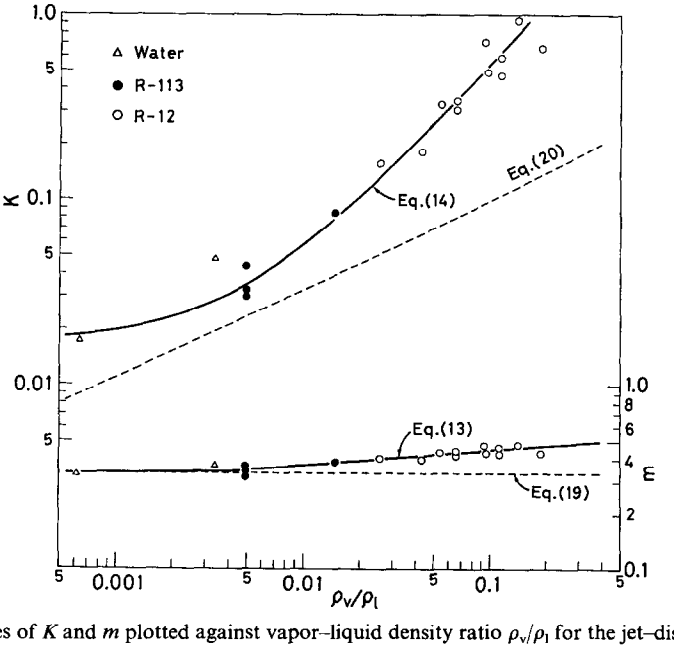

FIG. 5. Values of K and m plotted against vapor–liquid density ratio ρ_v/ρ_l for the jet–disk system.

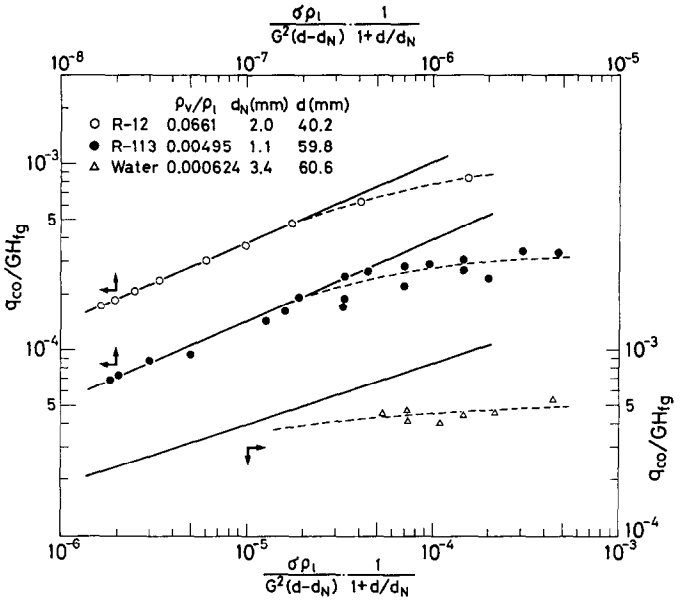

FIG. 6. Typical examples for applicable limit of correlations in the type of equation (12).

it has been tentatively assumed here that equation (7) applies to $\rho_v/\rho_l < 0.014$, while equation (8) to $\rho_v/\rho_l > 0.014$. According to the results of Table 2, any of the three correlations can predict CHF with rather good accuracies, though there are some differences between them.

(2) However, further comparisons must be made as to physical aspects in more detail. In order to do this, the following equation is taken as a common base:

$$\frac{q_{c0}}{GH_{fg}} = K'\left[\frac{\sigma\rho_l}{G^2(d-d_N)}\right]^{m'}. \tag{16}$$

First, Monde's equations (7) and (8) are compared with equation (16) to give

V: $m' = 0.343$, and

$$K' = 0.280\left(\frac{\rho_v}{\rho_l}\right)^{0.355}\frac{1}{(1+d/d_N)^{0.364}} \tag{7'}$$

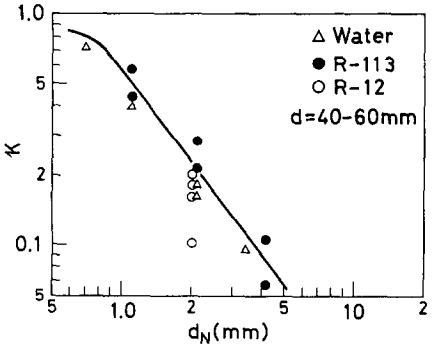

FIG. 7. Empirical presentation of k value.

I: $m' = 0.421$, and

$$K' = 0.925\left(\frac{\rho_v}{\rho_l}\right)^{0.534}\frac{1}{(1+d/d_N)^{0.303}}. \tag{8'}$$

Second, Sharan and Lienhard's equation (11) is compared with equation (16) to give

$$\left.\begin{aligned} m' &= A_2(r) \\ K' &= \left(0.00171+0.21\frac{\rho_v}{\rho_l}\right) \\ &\quad\times\left[1000\left(1-\frac{1}{d/d_N}\right)\right]^{A_2(r)}\frac{1}{(d/d_N)^{1/3}} \end{aligned}\right\} \tag{11'}$$

where $A_2(r)$ is given by equation (11) as a function of ρ_v/ρ_l. Finally, equation (12) in the present study is compared with equation (16) to give

$$m' = m, \quad \text{and} \quad K' = K/(1+d/d_N)^m \tag{12'}$$

where m and K are given by equations (13) and (14), respectively.

Equations (7'), (8'), (11') and (12') are compared with each other in Fig. 8 for the case of $d/d_N = 5$. Even if the value of d/d_N is as high as 50, the general aspect of Fig. 8 does not change so much. It is noted from Fig. 8 that, regarding the values of m' and K', either the Monde or the Sharan and Lienhard correlation suffers more or less with deviations from the trend of experimental data, because thick solid lines in Fig. 8 are ones transferred rather directly by equation (12') from the thick solid lines in Fig. 5 which agree well with experimental results.

(3) Regarding the effect of diameter ratio d/d_N on CHF, equation (11) seems quite different in character from equation (12). However, the form of equation

Table 2. Average (AVG) and root-mean-square (RMS) errors with various predictions

Fluid	ρ_v/ρ_l	NUM†		Monde equations (7) and (8)	Sharan equation (11)	Present work equations (12)–(14)
Water	0.000624	219	AVG‡	−3.01	2.49	1.89
			RMS	10.70	10.53	10.47
R-113	0.00495	183	AVG	18.42	9.68	−4.91
			RMS	31.32	24.10	21.38
R-12	0.0257	148	AVG	−7.79	−1.24	2.09
	−0.189		RMS	12.59	10.59	13.89
All data	0.000624	564	AVG	2.74	3.75	−0.54
	−0.189		RMS	20.17	16.29	15.69

† NUM represents total number of data.
‡ Both average and r.m.s. errors are presented in percentages.

(11) can be readily derived from equation (12) as follows. First, equation (12) is rewritten as

$$\frac{q_{c0}}{GH_{fg}}\left[\frac{d}{d_N}\left\{1-\left(\frac{d_N}{d}\right)^2\right\}\right]^m = K\left(\frac{\sigma\rho_l}{G^2 d}\right)^m. \quad (17)$$

Table 1 indicates that the existing data of CHF under normal conditions are within the range of $d/d_N = 3.9$–54.1, accordingly $1-(d_N/d)^2$ on the left-hand side of equation (17) can be approximated as unity within errors less than 6.6%. On the other hand, it is noted from Fig. 5 that, roughly speaking, the value of m in equation (17) takes values near 1/3. Hence, if m on the left-hand side of equation (17) is approximated as 1/3 leaving the right-hand side intact to give a space for empirical adjustments, equation (17) reduces to

$$\frac{q_{c0}}{GH_{fg}}\left(\frac{d}{d_N}\right)^{1/3} = K\left(\frac{\sigma\rho_l}{G^2 d}\right)^m. \quad (18)$$

This is nothing but the form of Sharan and Lienhard's equation (11).

(4) Equation (6) is a theoretical result derived through the concept of Critical Liquid Film Thickness with a model that the disk surface is fed with liquid through the circular periphery of 'the impinging zone' of a liquid jet. If equation (6) is compared with equation (12), it gives

$$m = 1/3 \quad (19)$$

$$K = 0.278(\rho_v/\rho_l)^{0.467}(1+\rho_v/\rho_l)^{1/3}. \quad (20)$$

Equations (19) and (20) are illustrated by broken lines in Fig. 5, respectively. It may be of interest to note that they do not agree well with experimental results, but still show rough coincidence in tendency with the data.

On the other hand, ref. [19] recently analyzed the

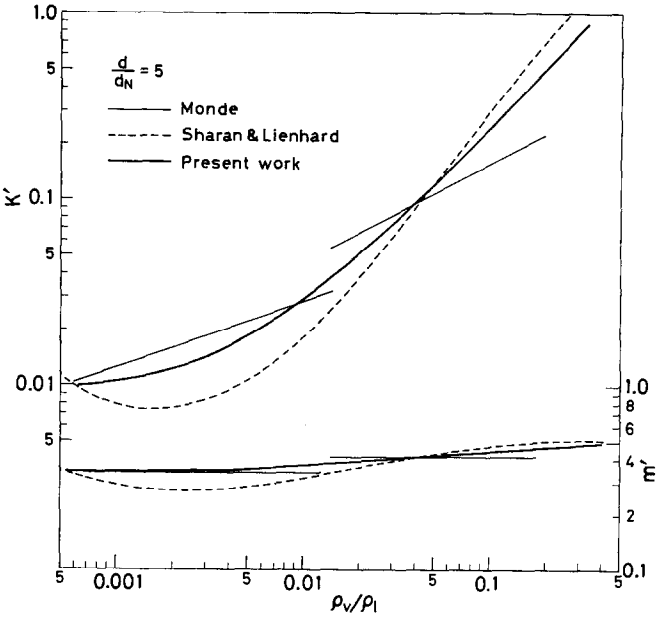

FIG. 8. Comparison between the Monde, the Sharan and Lienhard, and the present correlation of CHF.

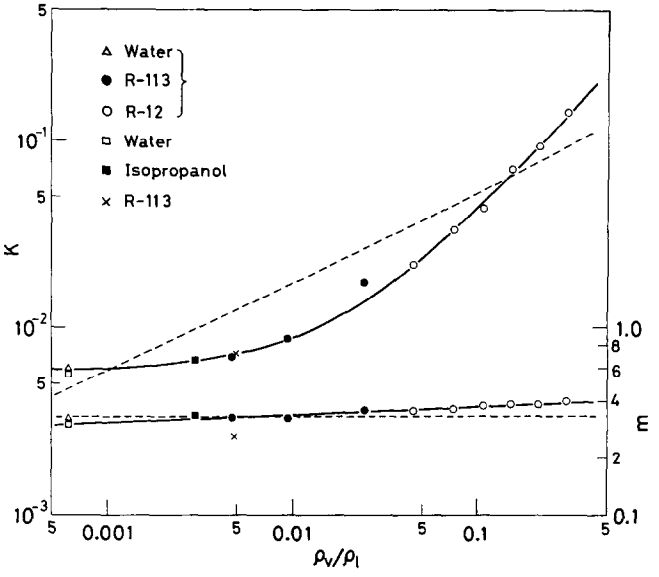

FIG. 9. Variation of K and m values with ρ_v/ρ_l for CHF on a cylinder in cross flow.

experimental data of CHF on a heated cylinder of diameter d in saturated cross flow of mass velocity G, and presented the results of Fig. 9 as to the values of K and m in the following correlation:

$$\frac{q_{c0}}{GH_{fg}} = K\left(\frac{\sigma\rho_l}{G^2 d}\right)^m. \tag{21}$$

Broken lines in Fig. 9 are the theoretical results for K and m, which have been derived through the concept of Critical Liquid Film Thickness and a model that the cylinder surface is fed with liquid from bulk liquid flow at the location of 'the stagnation point'.

The appearance of main flow configuration is quite different between the jet–disk and the cross flow system. However, the similarity in the nature of CHF observed in Figs. 5 and 9 strongly suggests that CHF in the above-mentioned two boiling systems may appear through rather similar mechanisms, basically at least.

4. CONCLUSIONS

(1) The existing data of CHF measured for the jet–disk system under normal conditions have been analyzed, covering the ranges of density ratio $\rho_v/\rho_l = 0.000624$–0.189, jet velocity $u = 0.3$–60.0 m s^{-1}, disk diameter $d = 10.0$–60.1 mm, nozzle diameter $d_N = 0.7$–4.1 mm, and diameter ratio $d/d_N = 3.9$–53.9. As the result, the following generalized correlation of CHF data is derived:

$$\frac{q_{c0}}{GH_{fg}} = K\left[\frac{\sigma\rho_l}{G^2(d-d_N)}\frac{1}{1+d/d_N}\right]^m$$

where

$$K = 0.0166 + 7.00(\rho_v/\rho_l)^{1.12}$$

$$m = 0.374(\rho_v/\rho_l)^{0.0155} \quad \text{for } \rho_v/\rho_l \leqslant 0.00403$$

$$m = 0.532(\rho_v/\rho_l)^{0.0794} \quad \text{for } \rho_v/\rho_l \geqslant 0.00403.$$

(2) If the jet velocity is reduced excessively under a fixed condition of other factors, CHF value begins to deviate from the normal state which is connected with the above-mentioned correlation. The value of (q_{c0}/GH_{fg}) at the transition point, that is the applicable limit of the foregoing correlation, can be roughly estimated by the following equation, as far as the existing data are concerned at least:

$$(q_{c0}/GH_{fg})_{trans.} = k/(d/d_N)^2$$

where k value is given by a curve in Fig. 7.

(3) In spite of the great difference in the appearance of the main flow configuration, the impinging jet and the cross flow system have similarities in characteristics of CHF, which suggests that CHF may appear basically through similar mechanisms in these systems.

Acknowledgement—The authors are extremely grateful to Professor M. Monde for his permission to use a lot of data which have so far been collected.

REFERENCES

1. Y. Katto and M. Kunihiro, Study of the mechanism of burn-out in boiling system of high burn-out heat flux, *Bull. J.S.M.E.* 1357–1366 (1973).
2. Y. Katto and M. Monde, Study of mechanism of burn-out in a high heat-flux boiling system with an impinging jet, *Proc. 5th Int. Heat Transfer Conf.*, Vol. IV, pp. 245–249 (1974).
3. M. Monde and Y. Katto, Burnout in a high heat-flux boiling system with an impinging jet, *Int. J. Heat Mass Transfer* **21**, 295–305 (1978).
4. Y. Katto and M. Shimizu, Upper limit of CHF in the saturated forced convection boiling on a heated disk

with a small impinging jet, *Trans. ASME*, Series C, *J. Heat Transfer* **101,** 265–269 (1979).
5. M. Monde, Burnout heat flux in saturated forced convection boiling with an impinging jet, *Heat Transfer—Jap. Res.* **9**(1), 31–41 (1980).
6. M. Katsuta, A study on boiling heat transfer in thin liquid film (6th Report, Case of R-113), *Proc. 14th Natl Heat Transfer Symp.*, Japan, pp. 154–157 (1980).
7. M. Katsuta and T. Kurose, A study on boiling heat transfer in thin liquid film (2nd Report, As for the critical heat flux of nucleate boiling), *Trans. J.S.M.E.* **47B,** 1849–1860 (1981).
8. M. Monde, H. Kusuda and O. Nagae, Critical heat flux of saturated forced convective boiling with an impinging jet, *Proc. 19th Natl Heat Transfer Symp.*, Japan, pp. 469–498 (1982).
9. M. Monde and Y. Okuma, Critical heat flux in saturated forced convective boiling on a heated disk with an impinging jet—CHF in *L*-regime, *Int. J. Heat Mass Transfer* **28,** 547–552 (1985).
10. M. Monde, Critical heat flux in saturated forced convection boiling on a heated disk with an impinging jet, *Trans. ASME*, Series C, *J. Heat Transfer* **109,** 991–996 (1987).
11. Y. Haramura and Y. Katto, A new hydrodynamic model of critical heat flux, applicable widely to both pool and forced convection boiling on submerged bodies in saturated liquids, *Int. J. Heat Mass Transfer* **26,** 389–399 (1983).
12. Y. Katto, Critical heat flux. In *Advances in Heat Transfer* (Edited by J. P. Hartnett and T. F. Irvine, Jr.), Vol. 17, p. 20. Academic Press, Orland (1985).
13. M. Monde, Critical heat flux in saturated forced convective boiling on a heated disk with an impinging jet, *Wärme- und Stoffübertr.* **19,** 205–209 (1985).
14. J. H. Lienhard and R. Eichhorn, Peak boiling heat flux on cylinders in a cross flow, *Int. J. Heat Mass Transfer* **19,** 1135–1142 (1976).
15. J. H. Lienhard and R. Eichhorn, On predicting boiling burnout for heaters cooled by liquid jets, *Int. J. Heat Mass Transfer* **22,** 774–776 (1979).
16. J. H. Lienhard and M. Z. Hasan, Correlation of burnout data for disk heaters cooled by liquid jets, *Trans. ASME*, Series C, *J. Heat Transfer* **101,** 383–384 (1979).
17. A. Sharan and J. H. Lienhard, On predicting burnout in the jet–disk configuration, *Trans. ASME*, Series C, *J. Heat Transfer* **107,** 398–401 (1985).
18. M. Monde, Private communication.
19. Y. Katto, S. Yokoya, S. Miake and M. Taniguchi, Critical heat flux on a uniformly heated cylinder in a cross flow of saturated liquid over a very wide range of vapor-to-liquid density ratio, *Int. J. Heat Mass Transfer* **30,** 1971–1977 (1987).

FLUX THERMIQUE CRITIQUE SUR UN DISQUE REFROIDI PAR UN JET CIRCULAIRE DE LIQUIDE SATURE FRAPPANT SON CENTRE

Résumé—On analyse les données disponibles de flux thermique critique (CHF) sur un disque refroidi par un jet liquide et on présente une formule générale qui couvre le rapport de densité vapeur–liquide $\rho_v/\rho_l = 0{,}000624$–$0{,}189$ et celui des diamètres disque-tuyère $d/d_N = 3{,}9$–$53{,}9$. Une méthode empirique est présentée pour estimer la limite à laquelle le CHF commence à s'écarter de l'état normal. Finalement, on montre que le système du disque avec un jet impactant a des similitudes avec le cas d'un cylindre chaud dans un écoulement transversal.

KRITISCHE WÄRMESTROMDICHTE EINER BEHEIZTEN SCHEIBE, DIE VON EINEM KREISRUNDEN STRAHL GESÄTTIGTER FLÜSSIGKEIT GEKÜHLT WIRD

Zusammenfassung—Die vorhandenen Daten für die kritische Wärmestromdichte (CHF) an einer scheibenförmigen Heizung, die durch einen Flüssigkeitsstrahl gekühlt wird, werden analysiert. Es wird eine verallgemeinerte Korrelation der Daten vorgestellt, welche das Dampf-Flüssigkeits-Dichteverhältnis $\rho_v/\rho_l = 0{,}000624$–$0{,}189$ und das Durchmesserverhältnis der Scheibe zur Düse $d/d_N = 3{,}9$–$53{,}9$ abdeckt. Es wird auch eine empirische Methode präsentiert, um die Grenzen zu bestimmen, wenn CHF vom normalen Zustand abweicht. Letztlich wird gezeigt, daß das System der scheibenförmigen Heizung mit einem auftreffenden Flüssigkeitsstrahl Ähnlichkeiten mit einem beheizten Zylinder in einer Querströmung aufweist.

КРИТИЧЕСКИЙ ТЕПЛОВОЙ ПОТОК НА ДИСКОВОМ НАГРЕВАТЕЛЕ, ОХЛАЖДАЕМОМ КРУГЛОЙ СТРУЕЙ ЖИДКОСТИ, УДАРЯЮЩЕЙСЯ О ЦЕНТР

Аннотация—Анализируются имеющиеся данные по критическому тепловому потоку (КТП) на дисковом нагревателе, охлаждаемом струей жидкости; представлена обобщенная зависимость результатов, охватывающая отношение плотностей системы пар–жидкость $\rho_v/\rho_e = 0{,}000624$–$0{,}189$ и отношение диаметров диска и сопла $d/d_N = 3{,}9$–$53{,}9$. Предел, при котором КТП начинает отклоняться от нормального состояния, оценивается эмпирическим методом. В результате показано, что система дисковый нагреватель-ударяющаяся струя сходна по характеру КТП с нагреваемым цилиндром в поперечном потоке.